Quaternary Science Reviews 111 (2015) 72–80

Contents lists available at ScienceDirect

Quaternary Science Reviews

journal homepage: www.elsevier.com/locate/quascirev

Revisiting tectonic corrections applied to Pleistocene sea-level highstands

Jessica R. Creveling [a, *], Jerry X. Mitrovica [b], Carling C. Hay [b, c], Jacqueline Austermann [b], Robert E. Kopp [c, d]

[a] Division of Geological and Planetary Sciences, California Institute of Technology, 1200 E. California Blvd., Pasadena, CA 91125, USA
[b] Earth and Planetary Sciences, Harvard University, 20 Oxford Street, Cambridge, MA 02138, USA
[c] Earth and Planetary Sciences, Rutgers University, 610 Taylor Road, Piscataway, NJ 08824, USA
[d] Rutgers Energy Institute, Rutgers University, 71 Dudley Road, New Brunswick, NJ 08901, USA

ARTICLE INFO

Article history:
Received 9 September 2014
Received in revised form
5 January 2015
Accepted 6 January 2015
Available online 3 February 2015

Keywords:
Ice age
Sea level
Tectonics
Interglacial
Ice volumes
Geophysical modeling

ABSTRACT

Tectonic displacement contaminates estimates of peak eustatic sea level (and, equivalently, minimum continental ice volumes) determined from the elevation of Quaternary interglacial highstand markers. For sites at which a stratigraphic or geomorphic marker of peak Marine Isotope Stage (MIS) 5e sea level exists, the standard approach for estimating local tectonic uplift (or subsidence) rates takes the difference between the elevation of the local highstand marker and a reference MIS 5e eustatic value, commonly chosen as +6 m, and divides by the age of the marker. The resulting rate is then applied to correct the elevation of all other local observed sea-level markers for tectonic displacement, including peak highstands of different ages (e.g., MIS 5a, MIS 5c and MIS 11), under the assumption that the tectonic rate remained constant over those periods. This approach introduces two potentially significant errors. First, the peak eustatic value adopted for MIS 5e in most previous studies (i.e., +6 m) is likely incorrect. Second, local peak sea level during MIS 5e is characterized by significant departures from eustasy due to glacial isostatic adjustment in response to both successive glacial–interglacial cycles and excess polar ice-sheet melt relative to present day values. We use numerical models of glacial isostatic adjustment that incorporate both of these effects to quantify the plausible range of the combined error and show that, even at sites far from melting ice sheets, local peak sea level during MIS 5e may depart from eustasy by 2–4 m, or more. We also demonstrate that the associated error in the estimated tectonic rates can significantly alter previous estimates of peak eustatic sea level during Quaternary highstands, notably those associated with earlier interglacials (e.g., MIS 11).

1. Introduction

The relationship between temperature change and ice-volume fluctuations during Pleistocene glacial–interglacial cycles provides an important measure of the sensitivity of the Earth system to climate change (Shackleton, 2000). Inferences of past ice volume derive from analysis of marine and ice-core oxygen isotopic depth series (Shackleton, 2000; Siddall et al., 2003) and various stratigraphic and geomorphic markers of local sea level. Local reconstructions of peak sea level during past interglacials, including MIS 5e (~125 ka) and MIS 11 (~410 ka), suggest at least partial collapse of both the Greenland Ice Sheet and the West Antarctic Ice Sheet during these periods of ice-age warmth (Neumann and Hearty, 1996; Hearty et al., 2007; Blanchon et al., 2009; Kopp et al., 2009, 2013; Muhs et al., 2011; Dutton and Lambeck, 2012; Raymo and Mitrovica, 2012; Roberts et al., 2012; O'Leary et al., 2013). The robustness of stratigraphic- and geomorphic-based sea-level inferences, however, depends on the accuracy with which these markers can be corrected for the complicating effect of tectonic uplift or subsidence.

A variety of processes contribute to local tectonic uplift and subsidence. At convergent plate margins, accretion, thrusting and/or thickening of the crust drive local uplift (Cawood et al., 2009); similar mechanisms occur along strike-slip boundaries oblique to plate motion (Basile and Allemand, 2002). Hotspots variably drive uplift or subsidence depending on the buoyancy force relative to

* Corresponding author.
E-mail address: jcrevel@gps.caltech.edu (J.R. Creveling).

http://dx.doi.org/10.1016/j.quascirev.2015.01.003
0277-3791/

the surrounding mantle. Likewise, passive margins undergo uplift or subsidence driven by ambient mantle convective forces, though typically (but not necessarily) on timescales longer than a glacial–interglacial cycle (Moucha et al., 2008; Müller et al., 2008; Spasojević et al., 2008; Rowley et al., 2013).

For sites that preserve an MIS 5e sea-level highstand marker, a standard method for estimating the rate of local tectonic uplift (or subsidence) computes the difference between the observed elevation of the MIS 5e marker and a reference eustatic (i.e., global mean) sea-level height for this time, typically chosen as ~6 m, and then divides this height difference by the age of the MIS 5e highstand (e.g., Broecker et al., 1968; Bloom et al., 1974; Dodge et al., 1983; Chappell and Shackleton, 1986; Ota and Omura, 1992; Gallup et al., 2002; Hearty, 2002; Speed and Cheng, 2004; Muhs et al., 2012a, among many others). Assuming that this rate remains constant through time, it is then applied to correct the elevation of all other observed sea-level markers at this site for tectonic uplift.

The precise origin of +6 m as an accepted value for MIS 5e peak eustatic sea level remains a topic of debate (see Murray-Wallace and Woodroffe, 2014 for a recent discussion). Hearty et al. (2007) attributed the correction to Neumann and Moore (1975) who reported a 5.9 m notch at a site in the northern Bahamas that they assumed was tectonically stable. However, earlier workers adopted the +6 m correction to estimate uplift rates, including both Broecker et al. (1968) in their study of Barbados and Bloom et al. (1974) in their analysis of records from Huon Peninsula (see also Chappell, 1974). Murray-Wallace and Belperio (1991) argued that the +6 m correction dates to the work of Veeh (1966), who estimated highstand values in the range +2–9 m on the basis of coral records from (purportedly) tectonically stable sites in both the Pacific and Indian Oceans. While Veeh (1966) was clearly an influential study, the adoption of +6 m by Bloom et al. (1974) and others may also have been influenced by a number of studies dating to the same period that inferred a MIS 5e peak eustatic sea level between 2 and 10 m (e.g., Broecker and Thurber, 1965; Thurber et al., 1965; Veeh, 1966; Land et al., 1967; Broecker and van Donk, 1970). Thus, the specific value of +6 m, originally adopted as representative of the above range of MIS 5e eustatic values, has been reinforced by numerous subsequent field studies at sites thought to be tectonically stable (e.g., Harmon et al., 1981; Brasier and Donahue, 1985; Jones and Hunter, 1990; Muhs et al., 2011), and it has evolved into a reference value commonly invoked without the associated uncertainty identified in earlier studies.

There are, of course, important exceptions. Some studies applied the same methodology for estimating tectonic uplift rates, but adopted a different value, or range of values, for the peak eustatic sea level during MIS 5e (Murray-Wallace, 2002; Schellmann and Radtke, 2004; Omura et al., 2004; Potter et al., 2004; Schellmann et al., 2004; Dumas et al., 2006; Bowen, 2010; Muhs et al., 2012b, 2014). These studies up to and including 2010 all considered values less than or equal to +6 m, reflecting the prevailing view that +6 m was an upper bound on MIS 5e peak eustatic sea level. Recent studies by two independent groups, however, concluded that MIS 5e peak eustatic sea level was ~6–9 m (Kopp et al., 2009, 2013; Dutton and Lambeck, 2012). Kopp et al. (2013) performed a statistical analysis of globally distributed MIS 5e geologic markers and marine oxygen isotope records and concluded that peak eustatic sea level during MIS 5e was extremely likely (95% probability) greater than 6.4 m but was unlikely (33% probability) to have exceeded 8.8 m. Dutton and Lambeck (2012) focused on a small set of high quality MIS 5e sea-level histories from Western Australia and the Seychelles and estimated peak eustatic sea level in the range 5.5–9 m. However, Hay et al. (2014) pointed out that the upper bound on the range cited by Dutton and Lambeck (2012), derived from the Seychelles record, does not account for the geographic variability in sea-level change associated with ice-sheet collapse (see below), and revised this bound downward to 7.5 m. The emerging view that +6 m represents a *lower* bound on MIS 5e peak eustatic sea level motivated Muhs et al. (2012b, 2014) to consider values of 6 and 9 m in estimating tectonic uplift rates for records from Curaçao and the Canary Islands, respectively.

Two potentially important errors are introduced in estimating a tectonic signal by subtracting a reference eustatic value from a local MIS 5e highstand marker. First, as discussed above, the adopted reference value may be in error. Second, an observed (local) MIS 5e highstand marker should not be corrected using the peak global eustatic value, but rather for a value that reflects the combined effect of eustasy and glacial isostatic adjustment (GIA) specific to that location. GIA encompasses the full deformational, gravitational, and rotational perturbation in sea level driven by the redistribution of ice and ocean mass, and introduces significant geographic variability (i.e., departures from eustasy) into the correction (Milne and Mitrovica, 2008; Dutton and Lambeck, 2012; Lambeck et al., 2012; O'Leary et al., 2013; Hay et al., 2014). The incorrect assumption that a globally averaged sea-level value can be used to correct local sea-level records or, equivalently, that the difference between the two is negligible, pervades the analyses cited above.

In this paper, we adopt geophysical models of GIA consistent with the observationally inferred bounds on peak eustatic sea level during MIS 5e to explore the potential error incurred in estimating tectonic effects on the basis of a simple eustatic correction to local MIS 5e highstand markers. We begin with a brief discussion of the basic physics underlying the departure of local, post-glacial sea level from eustasy. We then consider the impact of the assumption of eustasy on estimates of tectonic rates at the specific sites considered in the above analyses.

2. Methods

Our numerical predictions adopt a gravitationally self-consistent sea-level theory that accounts for the viscoelastic deformation of a spherically symmetric, Maxwell viscoelastic Earth, time-dependent shoreline migration, and the effects of Earth rotation changes on sea level (Kendall et al., 2005). The calculations require, as input, models for both Earth's viscoelastic structure and the evolving ice cover. For the former, we adopt the seismic model PREM to prescribe the elastic and density structure (Dziewonski and Anderson, 1981). We also adopt a radial profile of mantle viscosity defined by a very high viscosity (essentially elastic) lithosphere of thickness 95 km, an upper mantle viscosity of 0.5×10^{21}Pa s, and a lower mantle viscosity of 10^{22}Pa s. This model of mantle viscosity is consistent with a suite of inferences based on GIA data (Lambeck et al., 1998; Mitrovica and Forte, 2004).

Our synthetic ice history is comprised of two components. The first component of the ice history, which assumes that there is no difference in ice volume between the Last Interglacial (LIG; MIS 5e) and the present interglacial, isolates what one might call a background ice-age (i.e., glacial–interglacial) cycle signal. The geographic variability in sea-level change associated with this signal has been the focus of several recent GIA studies of MIS 5e (Dutton and Lambeck, 2012; Lambeck et al., 2012; O'Leary et al., 2013). (See also Raymo and Mitrovica, 2012, for analogous modeling of the background glacial–interglacial cycle signal associated with MIS 11). We adopt the ICE-5G version 1.2 model of the last glacial–interglacial cycle (Peltier, 2004), but slightly modify this ice history such that the cycle extends from 120 ka to present day. We then construct a penultimate glacial–interglacial cycle by duplicating the ICE-5G history and shifting it back in time so that

the Last Interglacial begins at 127 ka. Thus the model MIS 5e interglacial extends from 127 to 120 ka. In our model (ICE-5G) history, the cessation of melting within the present interglacial began at 4 ka. We note that in the discussion below the term 'interglacial' is used to denote these periods with no change in ice volume in the model ice-age cycles.

The second component of the ice history introduces a phase of excess melting of polar ice sheets relative to present-day ice volumes. We treat two cases of polar ice-sheet collapse that yield peak eustatic sea-level signals consistent with the estimates for MIS 5e of Kopp et al. (2009, 2013) and Dutton and Lambeck (2012) following the revision by Hay et al. (2014). In both scenarios, we assume melting of all marine-based sectors of the West Antarctic Ice Sheet (WAIS), which yields a eustatic sea-level rise of 3.3 m (Bamber et al., 2009). Climate simulations of Greenland Ice Sheet (GIS) retreat during MIS 5e have yielded estimates of peak eustatic sea-level rise ranging from 0.4 m to 4.4 m (Otto-Bliesner et al., 2006; Robinson et al., 2011; Born and Nisancioglu, 2012; Stone et al., 2013). In our scenario #1, the collapse of the Greenland Ice Sheet (GIS) produces a sea-level rise of 2.0 m, while in scenario #2 GIS mass loss contributes 3.0 m. Scenario #2 also includes melting of marine-based sectors of the East Antarctic Ice Sheet equivalent to a eustatic sea-level rise of 1.0 m. Finally, both scenarios incorporate a geographically uniform sea-level rise of 0.7 m to account for melting of mountain glaciers and the steric effect of ocean thermal expansion.

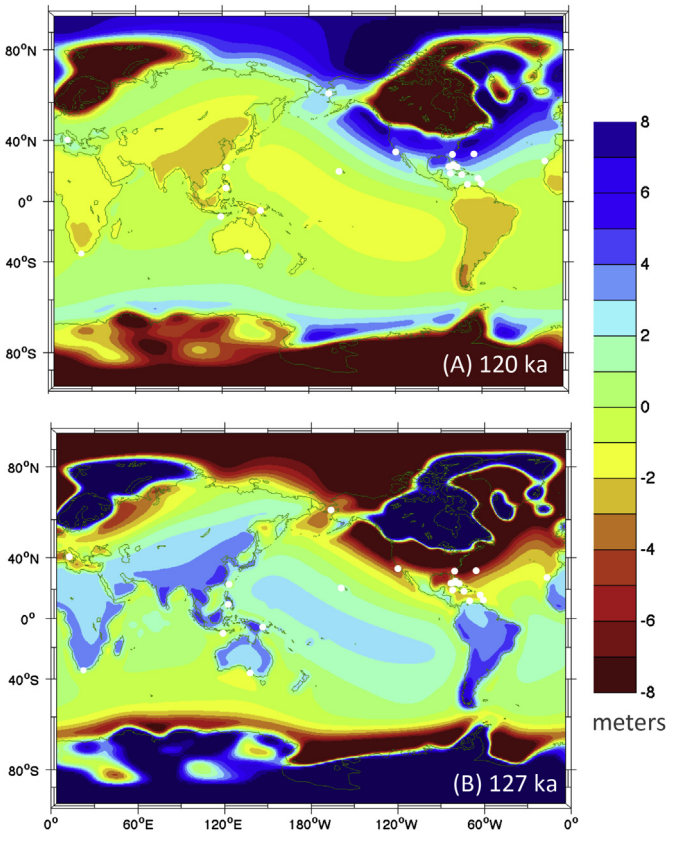

Fig. 1. Predicted departures from eustatic sea-level change due to glacial isostatic adjustment associated with the ice-age cycle. (A) The predicted elevation of a 120 ka MIS 5e interglacial highstand sea-level marker relative to the present day sea level (i.e., relative sea level) computed using the viscoelastic Earth model and two glacial-cycle ice-load history described in the text. (B) As in (A), except for the predicted elevation of a sea-level marker formed at the start of the modeled interglacial (127 ka). Since the ice load in this simulation has the same volume during MIS 5e and at present-day, the eustatic sea-level change is zero; thus, the average sea-level change over the global oceans is zero in both frames (A) and (B). Sites 1–22 listed in Table 1 are shown by small white dots on each frame.

The former has an upper bound value of about 0.4 m (Vaughan et al., 2013), and the latter has been estimated as 0.4 ± 0.3 m (McKay et al., 2011). We emphasize that the net effect of these two contributions is small; therefore, treating them as globally uniform will not introduce significant error into the results except in regions close to the mountain glaciers. Summing these various contributions yields a peak eustatic sea-level rise of 6 m for scenario #1 and 8 m for scenario #2.

While consensus is emerging with regard to the amplitude of MIS 5e peak eustatic sea level (Kopp et al., 2009, 2013; Dutton and Lambeck, 2012), there remains significant uncertainty as to the timing of this peak, with studies over several decades suggesting the possibility of multiple highstands (Bloom et al., 1974; Chappell, 1974; Stein et al., 1993; Blanchon et al., 2009; Thompson et al., 2011; Kopp et al., 2013). Accordingly, we consider two scenarios in which the excess melting takes place at either the beginning (127 ka) or the end (120 ka) of the modeled MIS 5e interglacial. It is important to emphasize that, regardless of the timing, this component of the ice history also contributes a sea-level signal with significant geographic variability (e.g., Hay et al., 2014).

3. Results

In the discussion below, we use the terms "ice-age cycle" signal and "excess melt" signal to refer to the two components of sea-level change discussed above. Further, the "eustatic" sea-level change is the globally averaged mean sea-level change after any marine-based sectors exposed by retreating ice have been filled with meltwater (Gomez et al., 2010). We use the term "GIA" signal to describe the combined effect of these three signals.

3.1. The ice–age cycle signal

In this section, we review how GIA resulting from the ice-age cycle results in local peak MIS 5e sea-level highstands that depart from eustasy. Fig. 1A and B show the predicted elevation of MIS 5e shorelines formed at the end (120 ka) and beginning (127 ka), respectively, of the modeled interglacial relative to present sea level (i.e., relative sea level) due to the background ice-age cycle signal. Deformational, gravitational, and rotational effects associated with the ice-age cycles contribute to these predictions, and we emphasize that there is no contribution from a change in ice volume between either of these times and the present. The physics underlying the prediction is well understood (Mitrovica and Milne, 2002; Lambeck et al., 2012) and we very briefly summarize it here, beginning with Fig. 1A.

Regions covered by ice sheets during the glacial cycles experience large-scale crustal rebound and sea-level fall during interglacials. Since our modeled MIS 5e interglacial persisted for longer than the duration of the current interglacial (i.e., 7 kyr, from 127 to 120 ka, compared to 4 kyr, from 4 to 0 ka), the predicted sea-level fall during the former was of greater amplitude than during the latter. Thus, the predicted elevation of a 120 ka shoreline at near-field locations (e.g., Hudson Bay) is tens of meters below present sea level (and off the color scale of the plot; Fig. 1A). In contrast, within the peripheral bulges of the Late Pleistocene ice complexes, for example along the US east coast, sea level rises during an interglacial as the bulges subside. Thus, a predicted 120 ka shoreline at these sites would lie above present-day sea level because Holocene interglacial sea level has not yet risen enough to reach these markers (Fig. 1A). Finally, in the far-field of the ice sheets, such as the equatorial Pacific, the simulation yields a low amplitude sea-level fall driven by ocean syphoning and continental levering (Nakada and Lambeck, 1989; Mitrovica and Milne, 2002). Since this fall is of greater magnitude during the (longer) modeled

MIS 5e interglacial than the current interglacial, the predicted elevation of 120 ka sea-level markers at far-field sites is up to ~2 m below present sea level (Fig. 1A).

Fig. 1B is a prediction of sea level at the start of the modeled MIS 5e interglacial relative to present day. The map has a geometry very close to Fig. 1A, but of opposite sign. The explanation for this change in sign is straightforward. As in Fig. 1A, the signal in Fig. 1B provides a measure of the difference in the predicted level of glacial isostatic adjustment at the earlier time (in this case, the start of the Last Interglacial) relative to the present-day. Consider, for example, a site on the peripheral bulge of the Laurentide Ice Sheet. Such a site is predicted to have experienced significantly more crustal subsidence (resulting in sea-level rise) at present day, ~4 kyr after the start of the current interglacial, than at the start of the Last Interglacial, and thus a 127 ka geological marker would be predicted to lie well below current sea level at this site. Similarly, the net far-field sea-level fall driven by ocean syphoning at present-day would be greater than at the start of the model MIS 5e, and in this case an ancient sea-level marker would lie above present sea level.

Recall that in the simulations shown in Fig. 1, eustatic sea level during the Last Interglacial is constrained to equal present-day eustatic sea level. Therefore, Fig. 1 quantifies one source of error in assuming that a reference eustatic value can be used to correct peak highstands of Last Interglacial age for the impact of glacial isostatic adjustment. Clearly, the level of error incurred from this assumption will depend on the age of the geological record marking peak sea level during MIS 5e and the proximity of a site to a melting ice sheet. However, even for sites within the far field of Pleistocene ice cover, the predicted departure from eustasy associated solely with the background ice-age cycle signal can reach up to ~±3 m (and somewhat larger at some far-field coastlines, e.g. southern South America).

3.2. The excess melt signal

The second contribution to the departure from eustasy results from the geographic variability of sea-level change following ice-sheet collapse during the Last Interglacial (the excess melt signal; Fig. 2). Fig. 2A and B show the predicted departure from eustasy driven by the excess melt scenarios #1 and #2 (prescribed above) 1 kyr after the ice-sheet collapse. Counterintuitively, rapid melting of an ice sheet leads to a fall in sea level within a few thousand kilometers of the ice sheet and a progressively increasing rise in sea level at greater distance (e.g., Mitrovica et al., 2001). This sea-level fall is due to the tandem effects of crustal rebound (which is largely elastic deformation across the 1 ka time window considered in Fig. 2A and B) and the diminution of the gravitational pull of the melting ice sheet on the ocean (rotational effects also contribute). Given the similarity in the loci of ice-sheet collapse, the geometry of the predicted sea-level change is similar in both Fig. 2A and B, although the magnitude varies as a result of the different prescribed peak eustatic sea level for each scenario. The predicted far-field sea-level rise above eustatic peaks at ~1.6 m and ~2.2 m for melt scenarios #1 and #2, respectively, or ~30% greater than the associated eustatic value. The sea-level fall close to the melting ice sheets has a peak amplitude that is an order of magnitude greater than the eustatic value. If one normalized Fig. 2A and B by their associated eustatic sea-level rise, the figures would show minor differences in the far-field, but large differences in the near-field of the melt zones (Antarctica and Greenland).

Fig. 2C and D show the predicted change in sea level 6 kyr after the excess melt scenarios #1 and #2, respectively. If the ice-sheet collapse occurred at the start of the modeled interglacial, then these figures represent the predicted signal near the end of model MIS 5e. Over this longer time scale, viscous effects reduce the amplitude of the far-field departure from eustasy by ~30% (a ~0.45 m difference in the peak far field value between Fig. 2A and C,

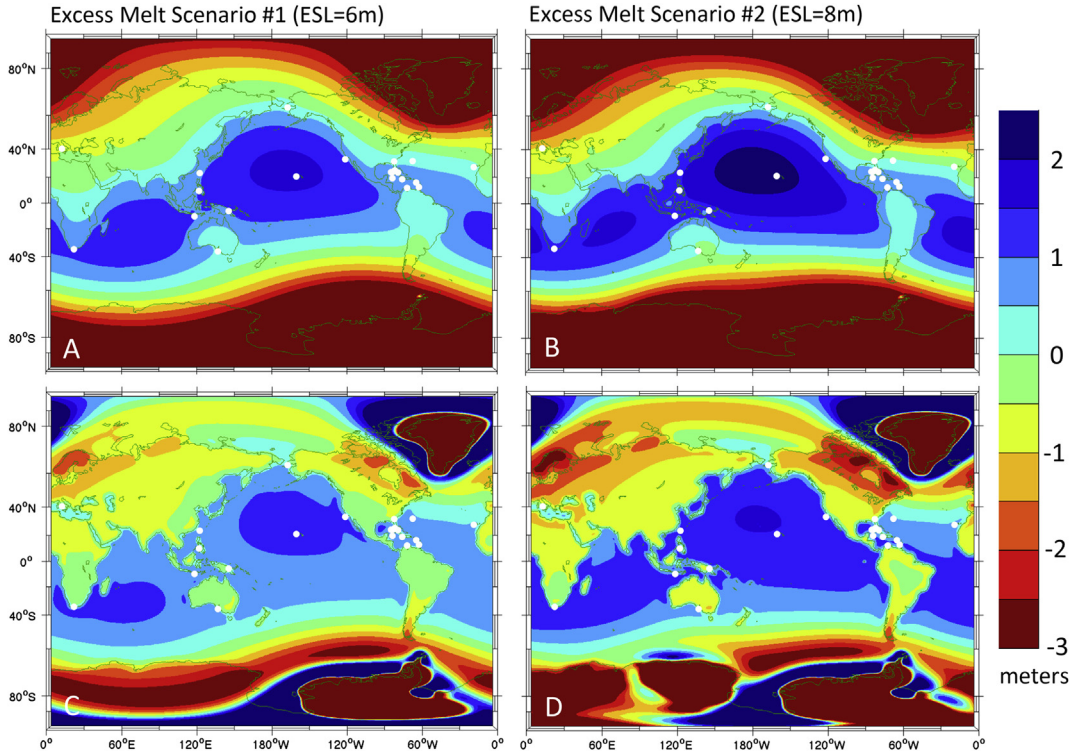

Fig. 2. Predicted departures from eustatic sea-level change 1 kyr after the excess melt scenarios #1 (A) and #2 (B). (C,D) as in (A) and (B), respectively, except the predicted departure from eustatic sea-level 6 kyr after the melt events. Melt scenario #1 (frames A,C) is characterized by eustatic sea-level rise of 6 m, while scenario #2 (frames B,D) has a eustatic sea-level rise of 8 m. Sites 1–22, listed in Table 1 and considered in Fig. 3, are shown by small white dots on each frame.

and ~0.7 m between Fig. 2B and D). Moreover, viscous effects alter the area of post-glacial uplift so that it more closely reflects the region of ancient ice cover. Viscous effects also introduce peripheral subsidence (and sea-level rise) surrounding this region of uplift (the peak values in both zones are off the scale of the plot).

3.3. The total GIA signal

The total sea-level signal due to GIA is the sum of three terms: the background ice-age cycle signal (Fig. 1), the excess melt signal (Fig. 2), and the eustatic signal. As is clear from the above discussion, the superposition of these signals will be characterized by significant geographic variability. Estimating the tectonic uplift rate from an observed MIS 5e peak highstand marker requires that one correct the elevation of the marker for the local GIA signal, not an assumed reference eustatic value. The error incurred by correcting with an assumed reference eustatic value equals the sum of the ice-age cycle and excess melt signals plus the difference between the actual peak eustatic value during MIS 5e and the adopted reference value. The error in the estimated tectonic uplift rate is given by dividing this error by the age of the MIS 5e highstand (~120 ka).

To explore this issue in more detail, Fig. 3 shows peak highstands (obtained at any time during the interglacial) predicted in four simulations in which the ice-age signal in Fig. 1 is augmented by an excess melt event associated with scenarios #1 and #2 (left and right columns of the figure, respectively) of duration 1 kyr occurring at either the start or end of the model MIS 5e interglacial (bottom and top rows of the figure, respectively). Results are shown for 22 sites taken from the literature reviewed in the Introduction. Sites 1–15, ordered (roughly) by progressive distance from the center of the ancient Laurentide Ice Sheet (see Fig. 1), represent locations in the vicinity of North, Central and South America, and the northeastern Atlantic (Canary Islands); site 16 (Rome/Lazio) is in Europe and relatively close to the location of the Fennoscandian Ice Sheet (see Fig. 1); and the remaining six sites represent locations in the far-field of the ancient ice cover. The results plotted on the figure are tabulated in Table 1, and the locations of the 22 sites are shown as white dots on each frame of Figs. 1 and 2.

Table 1
Predictions of peak MIS 5e highstand elevation.

Site name	Collapse Scenario#1 (6 m)		Collapse Scenario#2 (8 m)	
	End MIS 5e	Start MIS 5e	End MIS 5e	Start MIS 5e
1. Nome, Alaska	8.96	2.89	10.89	4.82
2. San Nicholas Is., CA	10.91	3.98	13.01	4.81
3. Charleston, SC	11.03	4.79	12.77	4.79
4. Bermuda	11.32	5.01	13.05	5.01
5. Berry Is., Bahamas	9.47	4.20	11.39	6.12
6. Eleuthera, Bahamas	9.63	3.90	11.56	5.83
7. North Key Largo, FL	9.08	4.83	11.02	6.77
8. Lower Florida Keys	9.21	4.54	11.16	6.50
9. Haiti	8.29	5.49	10.29	7.49
10. Cayman Islands	8.99	4.18	11.04	6.23
11. Barbuda	8.17	5.09	10.18	7.12
12. Barbados	7.63	4.96	9.71	7.04
13. Curaçao	6.93	6.06	9.00	8.13
14. Oahu	6.97	8.79	9.51	11.33
15. Canary Islands	6.45	4.77	8.23	6.55
16. Rome/Lazio	6.39	3.04	7.99	4.64
17. Hateruma Is., Japan	5.92	8.09	8.42	10.59
18. Panglao Is.	5.41	10.36	7.80	12.77
19. Huon Peninsula	5.53	9.75	7.77	11.98
20. Sumba, Indonesia	6.54	7.46	8.69	9.62
21. Coorong, Australia	5.33	7.89	6.92	9.49
22. Mossel Bay, S. Africa	5.70	9.11	8.00	11.41

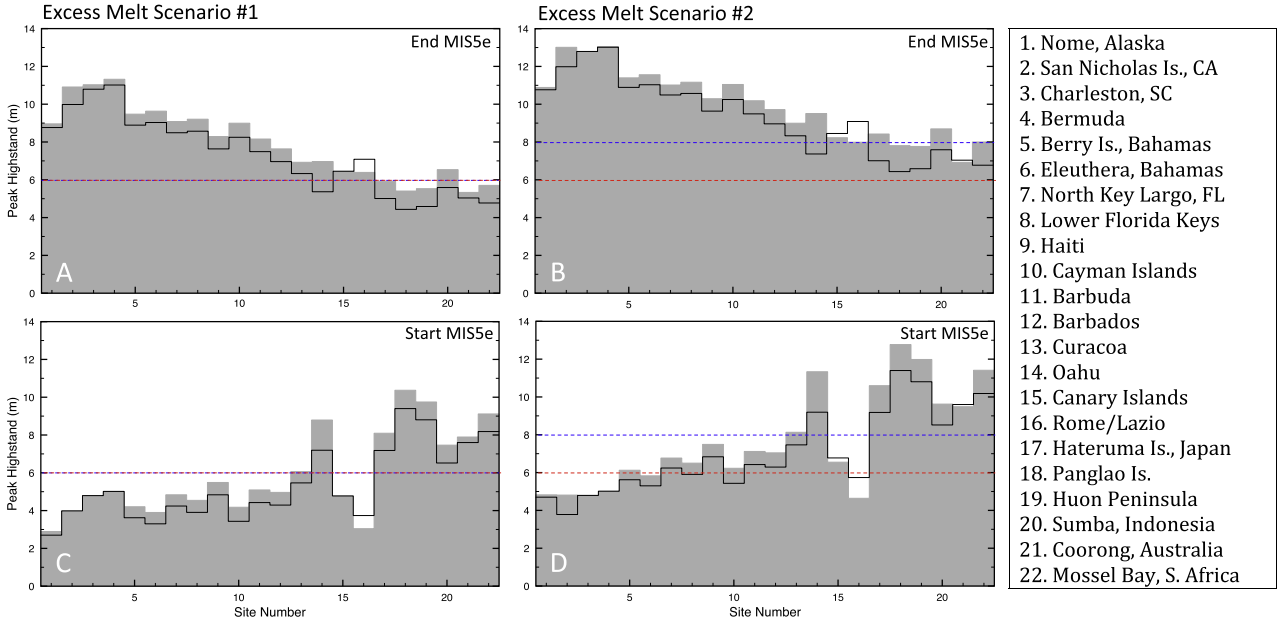

Fig. 3. Site-specific predictions of peak relative sea level during the model MIS 5e interglacial. The total signal (elevation of the shaded gray zone) incorporates the combined effect of the background ice-age signal plus the excess-melt signal introduced at either the start (bottom row) or end (top row) of the interglacial. The left and right columns are predictions based on the excess melt scenarios #1 and #2, respectively. The dashed blue line on each frame is the eustatic signal associated with these scenarios (6 m and 8 m, respectively). The thin dashed red line on each frame is the +6 m reference eustatic value for MIS 5e often adopted in calculations of site-specific tectonic rates (see references in the Introduction). The solid black line in each frame is the eustatic signal associated with the modeled ice sheet collapse (+6 m at left and +8 m at right) plus the background ice-age signal. The sea-level simulation is run across the last two glacial cycles (see text) and the value plotted is the peak sea level attained at any time during the model MIS 5e for the given simulation. Sites 1–22 are listed in the legend on the right of the figure, and each location is shown by a small white dot on Figs. 1 and 2. In frames C and D, the cases for which the total signal is exactly the same as the eustatic plus ice age signal (i.e., the black line and height of the shaded region coincide; sites 2–4 in frame C and sites 3–4 in frame D) indicate sites where the peak highstand is predicted to occur at the end of the model interglacial despite the fact that the collapse (and recovery) occur at the start of the interglacial. (For interpretation of the references to color in this figure legend, the reader is referred to the web version of this article.)

The dashed blue line on each frame is the eustatic signal associated with the ice collapse scenario adopted in the simulation, while the solid black line is the sum of this eustatic value plus the ice-age cycle signal. Adding the excess melt signal to the solid line yields the total GIA signal (the height of the shaded gray zone). As a point of comparison, the dashed horizontal red line on each frame is the +6 m value adopted as the peak eustatic value during MIS 5e, or as an upper bound on this peak value, in nearly all previous estimates of tectonic rates based on MIS 5e highstand observations (e.g., Broecker et al., 1968; Bloom et al., 1974; Dodge et al., 1983; Chappell and Shackleton, 1986; Ota and Omura, 1992; Gallup et al., 2002; Hearty, 2002; Murray-Wallace, 2002; Schellmann and Radtke, 2004; Omura et al., 2004; Potter et al., 2004; Schellmann et al., 2004; Speed and Cheng, 2004; Dumas et al., 2006; Bowen, 2010; Muhs et al., 2012a). The dashed blue and red lines on the frames at left in Fig. 3 are indistinguishable because the eustatic value adopted in excess melt scenario #1 is the same as the reference value, +6 m.

Whereas current estimates of the peak eustatic sea level during MIS 5e suggest a value somewhere in the range 6–8 m (Kopp et al., 2009, 2013; Dutton and Lambeck, 2012), there is as yet no consensus on the time history of the excess melt signal within the Last Interglacial (Thompson et al., 2011; Kopp et al., 2013). Thus, the difference between the elevation of the shaded gray zone in the four simulations and the adopted reference eustatic value for MIS 5e (as opposed to the actual eustatic value of the excess melt scenario) provides a plausible range for the error that has been incurred in previous estimates of the tectonic signal at these geographic sites.

Consider the simulation in which the excess melt event of scenario #1 (eustatic value = +6 m) occurs at the end of the model MIS 5e interglacial (Fig. 3A). This timing is consistent, for example, with the inference of O'Leary et al. (2013) based upon observations from western Australia. In this case, sites 1–12 are strongly influenced by the dynamics of the peripheral bulge encircling the ancient Laurentide Ice Sheet (Fig. 1A) and this ice-age cycle signal drives a departure from eustasy of ~1–5 m (Fig. 3A). The same 12 sites are within a region where the excess melt signal, dominated by the migration of water from the polar ice sheets, adds up to ~1 m to this departure (Fig. 2A). The net effect is that the total GIA signal exceeds the eustatic value by ~2–6 m at these sites (Fig. 3A). The prediction at Barbados (site 12) exceeds the eustatic signal adopted in the scenario #1 simulation by ~2 m. Indeed, one has to consider sites as far south as Curaçao (site 13) before the departure of the total GIA signal from eustatic value of the simulation is ~1 m or less.

The remaining sites all have a predicted GIA signal that is within ~1–1.5 m of the peak eustatic value (Fig. 3A). Of these, sites 17–22 are all well away from Late Pleistocene ice cover and the ice-age signal at these sites is negative, reflecting the influence of ocean syphoning (Fig. 1A). In contrast, the excess melt signal is positive because of the migration of water to the far field of the polar ice sheets (Fig. 2A), and this partially offsets the net departure from eustasy associated with the ice-age cycle signal.

Fig. 3B shows the case where the excess melt scenario #2 (Fig. 2B), with a peak eustatic value of 8 m, is applied at the end of the model MIS 5e interglacial. As one would expect, the total GIA signal in this case is shifted upwards by ~2 m relative to the analogous case for melt scenario #1. The shift is not precisely 2 m (Table 1), however, because the departure from eustasy associated with the predictions for scenarios #1 and #2 is similar in percentage, but not absolute terms. Thus the excess melt signal for scenario #2 at a given site tends to be somewhat higher than in scenario #1 (consider, for example, sites 10, 17 and 20). In any case, for sites 1–17 and 20, the error one would incur by assuming that local sea-level change was equal to a reference value of +6 m (i.e., the difference in the height of the shaded region and the red dashed line) is ~2 m greater in scenario #2 than in the scenario #1. For sites 18, 19, 21 and 22, the error changes sign and its magnitude increases to 1–2 m.

We next turn to the case of a 1 kyr pulse of ice-sheet collapse and recovery at the start of MIS 5e (Fig. 3C and D). In this case, the predicted peak highstand does not always occur at the start of the interglacial; at some sites on the periphery of the Laurentide Ice Sheet (e.g., 2–4 in Fig. 3C and 3–4 in Fig. 3D) the predicted sea-level rise across MIS 5e due to ice-age cycle loading is greater than the time-limited increase in sea level due to the early ice-sheet collapse, and thus the peak highstand is predicted to occur at the end of the modeled interglacial. Nevertheless, some general patterns in the predictions arise. For example, sites 1–12, on the peripheral bulge of the Laurentide Ice Sheet, have predicted peak values ~2 m lower than the eustatic value associated with the ice-sheet collapse. This discrepancy is largely associated with the ice-age cycle signal appropriate to the start of the interglacial, which is negative at these sites (Fig. 1B).

In contrast to the predictions for a late-stage ice-sheet collapse (Fig. 3A and B), the predicted peak highstands in the far field (e.g., sites 17–22) in the case of an early MIS 5e collapse (Fig. 3C and D) are characterized by a large departure (~2–4 m) from the eustatic value of the excess melting signal. At these sites, the ice-age cycle signal is dominated by ocean syphoning and it contributes a positive departure from eustasy (Fig. 1B). The ice-sheet collapse signal (either Fig. 2A or B) adds constructively to this departure.

We also considered a scenario in which the ice-sheet collapse occurred at the beginning of the model MIS 5e interglacial and that the collapse persisted until the end of the interglacial (see supplementary Fig. S1). The predicted relative sea level at the start of the interglacial is essentially the same as in the last scenario, but by the end of the model interglacial the excess melt signal evolves to the form of Fig. 2C and D, for scenarios #1 and #2, respectively. In this case, the predicted departure of the peak highstand from the eustatic value associated with the ice-sheet collapse is a mix of the results in Fig. 3; in particular, predictions for sites 1–12 resemble the top row of Fig. 3, while predictions for sites in the far field are similar to the bottom row of Fig. 3. The net effect is that the departure is relatively large at all 22 sites.

4. Discussion

We have presented predictions of peak highstand elevations for a series of GIA simulations that combine ice-sheet collapse scenarios with equivalent eustatic values of either +6 m or +8 m, timed to occur at either the start or end of a modeled MIS 5e interglacial, with a background signal associated with the ice-age cycles. Our predictions quantify the potential error incurred in studies that estimated local tectonic uplift rates by assuming that the GIA correction applied to observed MIS 5e highstands is geographically uniform and equal to some adopted reference eustatic value. The error in this assumption has three components: the departure from eustasy associated with (1) the background ice-age cycle signal and (2) the excess melt signal, as well as (3) the difference between the actual peak eustatic value during MIS 5e and the adopted reference value.

The 22 sites considered in Fig. 3 were selected from studies that inferred tectonic uplift rates from MIS 5e peak highstand observations in the manner described above, or that applied such rates to correct highstands dated to other periods of minimum ice volumes, including the MIS 11 interglacial and MIS 5a and 5c (e.g., Bloom et al., 1974; Dodge et al., 1983; Chappell and Shackleton, 1986; Ota and Omura, 1992; Gallup et al., 2002; Hearty, 2002; Murray-Wallace, 2002; Schellmann and Radtke, 2004; Omura et al., 2004;

Potter et al., 2004; Schellmann et al., 2004; Speed and Cheng, 2004; Dumas et al., 2006; Bowen, 2010; Muhs et al., 2012a). While not an exhaustive list, these 22 sites provide a measure of the plausible departure of the total GIA signal from eustasy at sites in the intermediate field (e.g., peripheral bulge) and far field of Late Pleistocene ice complexes, including the polar ice sheets.

From Fig. 3 we conclude that the magnitude of the total error in any MIS 5e-derived estimate of tectonic uplift rate is a function of the location of the site as well as the timing and magnitude of the ice-sheet collapse during MIS 5e. Moreover, the relative contribution of the three error sources listed above to the total error is similarly a function of these details. Thus, all three variables must be accounted for in any reanalysis of previous estimates of tectonic uplift rate. We note that the departure from eustasy associated with the background ice-age cycle, and the associated error, will be sensitive to the two primary inputs in the ice-age cycle calculations, namely the space-time geometry of ice sheets across the last two glacial–interglacial cycles (and, in particular, the last and penultimate deglaciation phases) and the viscosity structure of the Earth's mantle. In the analysis here, we have presented illustrative results for one ice history and one mantle viscosity model.

The error in applying the MIS 5e-derived tectonic rate estimated in the above manner to correct the elevation of an older or younger geological highstand (or lowstand) marker at the same site will be a function of the age of that marker. For example, a 1 m error in the tectonic signal inferred from a MIS 5e highstand will be magnified to a ~4 m error in the tectonic correction to a MIS 11 highstand from the same site, and will be scaled by factors of ~100/120 and ~80/120 if applied to correct MIS 5c and MIS 5a highstands, respectively.

As an illustration, consider the analysis of Bowen (2010), who corrected observed MIS 5e highstands at Charleston, Coorong, Curaçao, Nome, Rome, Barbados, and Sumba for peak eustatic values of +2 m, +4 m and +6 m. In estimating the local tectonic rate at each site, Bowen also considered ages for the MIS 5e highstand ranging from 116 ka to 132 ka. The tectonic uplift rates were used to calculate the amount of cumulative, long-term uplift in observed peak MIS 11 highstands at each site and to estimate, from the average residual at all sites, the peak eustatic sea level during this earlier interglacial. If we consider the middle of Bowen's age range for MIS 5e, then his estimates of peak eustatic sea level during MIS 11 were 0.5 m, 3 m and 8 m in the case of eustatic corrections to MIS 5e highstands of +2 m, +4 m and +6 m, respectively (see his Table 2).

We have repeated Bowen's (2010) analysis, but have replaced the aforementioned reference eustatic values he used to correct the observed MIS 5e highstands with the GIA predictions listed in Table 1. We emphasize that the four cases summarized in Table 1 are consistent with current bounds on peak eustatic sea level during MIS 5e (Kopp et al., 2009, 2013; Dutton and Lambeck, 2012) and incorporate realistic geographic variability in the GIA signal during MIS 5e. Using the GIA-corrected MIS 5e highstand elevations to estimate the tectonic rate at each site, applying these to the observed elevation of MIS highstands, and taking the mean, yields four estimates of peak eustatic sea level during MIS 11 that range from 8.5 m to 22.2 m, and average to 15.1 m. This example illustrates the sensitivity of estimates of peak MIS 11 sea level to the assumption that observed MIS 5e highstands can be corrected for GIA effects using a reference eustatic value.

As a second example, Muhs et al. (2014) inferred peak MIS 11 sea level on the basis of coral records from Curaçao and adopted paleo-sea-level values of +6 m and +9 m for the MIS 5e highstands at this site to calculate a local tectonic uplift rate. Our four simulations summarized in Table 1 yield GIA signals at Curaçao ranging from 6 m to 9 m, with a mean value of ~7.5 m. We conclude that the two values adopted by Muhs et al. (2014) provide a reasonable bound on the possible GIA correction to MIS 5e highstands appropriate for this site.

In highlighting the potential error introduced in previous estimates of tectonic corrections, our intent is not to advocate for specific models of either GIA or ice-sheet collapse during MIS 5e. Rather, our aim has been to explore the extent to which the total GIA signal at specific sites (including both the ice-age cycle signal and the signal from excess polar ice-sheet melt during MIS 5e) — even those sites well away from Pleistocene ice cover — can depart from the globally-averaged (eustatic) rate of sea-level change. As we have demonstrated, this departure, together with any error in the reference peak eustatic value adopted for MIS 5e, introduces a potentially large error in the estimated tectonic correction, an error sufficient to fundamentally alter estimates of eustatic sea level at other times of minimum ice volume, including MIS 5a, MIS 5c and MIS 11.

The accuracy of any alternate methodology for estimating tectonic uplift rates will depend on our ability to constrain the total GIA signal at various sites, which will in turn depend, in part, on the accuracy with which the geometry and timing of sea-level changes during MIS 5e can be constrained. One possible route forward would be to apply statistical methods (e.g., Kopp et al., 2009, 2013) to the global database of sea-level markers of MIS 5e age (e.g., coral reef terraces and biofacies, erosional wave-cut platforms, sedimentary facies, and isotopic measurements) to derive probabilistic and site-specific bounds on the total GIA contribution to peak MIS 5e highstands and, by implication, probabilistic bounds on the tectonic correction to these highstands. Such methods can be extended to include other data sets (e.g., relative sea-level markers of different age, and observations related to the Earth's gravity field and rotational state) that can provide additional constraints on the ice-age cycle signal.

Regardless of the method for estimating tectonic uplift rate, the pervasive, underlying assumption in ice-age sea level studies that the tectonic uplift rate is constant and uniform in the vicinity of a specific site, is also open to question given the evidence for earthquake cycle variability in elevation changes (e.g., Sieh et al., 2008) and large local gradients in tectonic rates (e.g., Barbados; Schellmann and Radtke, 2004; Radtke and Schellmann, 2006) at sites near plate boundaries. Both of these issues warrant future study.

Acknowledgments

This work was supported by an Agouron Institute Geobiology Postdoctoral Fellowship and Caltech Postdoctoral Fellowship in Geology (JRC), U.S. National Science Foundation grants ARC-1203414 and ARC-1203415 (JXM, CCH, REK) and Harvard University (JXM, JA). We thank Daniel Muhs for his comprehensive review and constructive suggestions in regard to an earlier version of this manuscript.

Appendix A. Supplementary data

Supplementary data related to this article can be found at http://dx.doi.org/10.1016/j.quascirev.2015.01.003.

References

Bamber, J.L., Riva, R.E.M., Vermeersen, L.L.A., LeBrocq, A.M., 2009. Reassessment of the potential sea-level rise from a collapse of the West Antarctic Ice Sheet. Science 324, 901–903.

Basile, C., Allemand, P., 2002. Erosion and flexural uplift along transform faults. Geophys. J. Int. 151, 646–653.

Blanchon, P., Eisenhauer, A., Fietzke, J., Liebetrau, V., 2009. Rapid sea-level rise and reef back-stepping at the close of the Last Interglacial highstand. Nature 458, 881–884.
Bloom, A.L., Broecker, W.S., Chappell, J.M.A., Matthews, R.K., Mesolella, K.J., 1974. Quaternary sea level fluctuations on a tectonic coast: new $^{230}Th/^{234}U$ dates from the Huon Peninsula, New Guinea. Quat. Res. 4, 185–204.
Born, B., Nisancioglu, K.H., 2012. Melting of Northern Greenland during the last interglaciation. The Cryosphere 6, 1239–1250.
Bowen, D.Q., 2010. Sea level ~400 000 years ago (MIS 11): analogue for present and future sea-level? Clim. Past 6, 19–29.
Brasier, M., Donahue, J., 1985. Barbuda – an emerging reef and lagoon complex on the edge of the Lesser Antilles island arc. J. Geol Soc. Lond. 142, 1101–1117.
Broecker, W.S., van Donk, J., 1970. Insolation changes, ice volumes, and the O-18 record in deep-sea cores. Rev. Geophys. Space Phys. 8, 169–198.
Broecker, W.S., Thurber, D.L., 1965. Uranium-series dating of corals and oolites from Bahamian and Florida Key limestones. Science 149, 58–60.
Broecker, W.S., Thurber, D.L., Goddard, J., Ku, T.-L., Matthews, R.K., Mesolella, K.J., 1968. Milankovitch hypothesis supported by precise dating of coral reefs and deep-sea sediments. Science 159, 297–300.
Cawood, P.A., Kröner, A., Collins, W.J., Kusky, T.M., Mooney, W.D., Windley, B.F., 2009. Accretionary Orogens through Earth History. In: Geol. Soc. Lond., Spec. Publ, vol. 318, pp. 1–36.
Chappell, J., 1974. Geology of coral terraces, Huon Peninsula, New Guinea: a study of Quaternary tectonic movements and sea-level changes. Geol. Soc. Am. Bull. 85, 553–570.
Chappell, J., Shackleton, N.J., 1986. Oxygen isotopes and sea level. Nature 324, 137–140.
Dodge, R.E., Fairbanks, R.G., Benninger, L.K., Maurrasse, F., 1983. Pleistocene sea levels from raised coral reefs of Haiti. Science 219, 1423–1425.
Dumas, B., Hoang, C.T., Raffy, J., 2006. Record of MIS 5 sea-level highstands based on U/Th dated coral terraces of Haiti. Quat. Int. 145–146, 106–118.
Dutton, A., Lambeck, K., 2012. Ice volume and sea level during the Last Interglacial. Science 337, 216–219.
Dziewonski, A.M., Anderson, D.L., 1981. Preliminary Reference Earth Model (PREM). Phys. Earth Planet. Inter. 25, 297–356.
Gallup, C.D., Cheng, H., Taylor, F.W., Edwards, R.L., 2002. Direct determination of the timing of sea level change during termination II. Science 295, 310–313.
Gomez, N., Mitrovica, J.X., Tamisiea, M.E., Clark, P.U., 2010. A new projection of sea level change in response to collapse of marine sectors of the Antarctic ice sheet. Geophys. J. Int. 180, 623–634.
Harmon, R.S., Land, L.S., Mitterer, R.M., Garrett, P., Schwarcz, H.P., Larson, G.J., 1981. Bermuda sea level during the Last Interglacial. Nature 289, 481–483.
Hay, C., Mitrovica, J.X., Gomez, N., Creveling, J.R., Austermann, J., Kopp, R.E., 2014. The sea-level fingerprints of ice-sheet collapse during interglacial periods. Quat. Sci. Rev. 87, 60–69.
Hearty, P.J., 2002. The Ka'ena highstand of O'ahu, Hawai'i: further evidence of Antarctic ice sheet collapse during the Middle Pleistocene. Pac. Sci. 56, 65–81.
Hearty, P.J., Hollin, J.T., Neumann, A.C., O'Leary, M.J., McCulloch, M., 2007. Global sea-level fluctuations during the Last Interglaciation (MIS 5e). Quat. Sci. Rev. 26, 2090–2112.
Jones, B., Hunter, I.G., 1990. Pleistocene paleogeography and sea levels on the Cayman Islands, British West Indies. Coral Reefs 9, 81–91.
Kendall, R.A., Mitrovica, J.X., Milne, G.A., 2005. On post-glacial sea level – II, Numerical formulation and comparative results on spherically symmetric models. Geophys. J. Int. 161, 679–706.
Kopp, R.E., Simons, F.J., Mitrovica, J.X., Maloof, A.C., Oppenheimer, M., 2009. Probabilistic assessment of sea level during the Last Interglacial stage. Nature 462, 863–867.
Kopp, R.E., Simons, F.J., Mitrovica, J.X., Maloof, A.C., Oppenheimer, M., 2013. A probabilistic assessment of sea level variations within the Last Interglacial stage. Geophys. J. Int. 193, 711–716.
Lambeck, K., Smither, C., Johnston, P., 1998. Sea-level change, glacial rebound and mantle viscosity for northern Europe. Geophys. J. Int. 134, 102–144.
Lambeck, K., Purcell, A., Dutton, A., 2012. The anatomy of interglacial sea levels: the relationship between sea levels and ice volumes during the Last Interglacial. Earth Planet. Sci. Lett. 315–316, 4–11.
Land, L.S., Mackenzie, F.T., Gould, S.J., 1967. The Pleistocene history of Bermuda. Geol. Soc. Am. Bull. 78, 993–1006.
McKay, N.P., Overpeck, J.T., Otto-Bliesner, B.L., 2011. The role of ocean thermal expansion in Last Interglacial sea level rise. Geophys. Res. Lett. 38, L14605. http://dx.doi.org/10.1029/2011GL048280.
Milne, G.A., Mitrovica, J.X., 2008. Searching for eustasy in deglacial sea-level histories. Quat. Sci. Rev. 27, 2292–2302.
Mitrovica, J.X., Forte, A.M., 2004. A new inference of mantle viscosity based upon joint inversion of convection and glacial isostatic adjustment data. Earth Planet. Sci. Lett. 225, 177–189.
Mitrovica, J.X., Milne, G.A., 2002. On the origin of Late Holocene sea-level highstands within equatorial ocean basins. Quat. Sci. Rev. 21, 2179–2190.
Mitrovica, J.X., Tamisiea, M.E., Davis, J.L., Milne, G.A., 2001. Recent mass balance of polar ice sheets inferred from patterns of global sea-level change. Nature 409, 1026–1029.
Moucha, R., Forte, A.M., Mitrovica, J.X., Rowley, D.B., Quéré, S., Simmons, N.A., Grand, S.P., 2008. Dynamic topography and long-term sea-level variations: there is no such thing as a stable continental platform. Earth Planet. Sci. Lett. 271, 101–108.
Muhs, D.R., Simmons, K.R., Schumann, R.R., Halley, R.B., 2011. Sea-level history of the past two interglacial periods: new evidence from U-series dating of reef corals from south Florida. Quat. Sci. Rev. 30, 570–590.
Muhs, D.R., Simmons, K.R., Schumann, R.R., Groves, L.T., Mitrovica, J.X., Laurel, D., 2012a. Sea-level history during the Last Interglacial complex on San Nicolas Island, California: implications for glacial isostatic adjustment processes, paleozoogeography and tectonics. Quat. Sci. Rev. 37, 1–25.
Muhs, D.R., Pandolfi, J.M., Simmons, K.R., Schumann, R.R., 2012b. Sea-level histories of past interglacial periods from uranium-series dating of corals, Curaçao, Leeward Antilles islands. Quat. Res. 78, 157–159.
Muhs, D.R., Meco, J., Simmons, K.R., 2014. Uranium-series ages of corals, sea level history, and palaeozoogeography, Canary Islands, Spain: an exploratory study for two Quaternary interglacial periods. Palaeogeogr. Palaeoclimatol. Palaeoecol. 394, 99–118.
Müller, R.D., Sdrolias, M., Gaina, C., Steinberger, B., Heine, C., 2008. Long-term sea-level fluctuations driven by ocean basin dynamics. Science 319, 1357–1362.
Murray-Wallace, C.V., 2002. Pleistocene coastal stratigraphy, sea-level highstands and neotectonism of the southern Australian passive continental margin – a review. J. Quat. Sci. 17, 469–489.
Murray-Wallace, C.V., Belperio, A.P., 1991. The Last Interglacial shoreline in Australia. Quat. Sci. Rev. 10, 441–461.
Murray-Wallace, C.V., Woodroffe, C.D., 2014. Quaternary Sea-level Changes: a Global perspective. Cambridge Univ. Press., p. 502
Nakada, M., Lambeck, K., 1989. Late Pleistocene and Holocene sea-level change in the Australian region and mantle rheology. Geophys. J. Int. 96, 497–517.
Neumann, A.C., Hearty, P.J., 1996. Rapid sea-level changes at the close of the Last Interglacial (stage 5e) recorded in Bahamian Island geology. Geology 24, 775–778.
Neumann, A.C., Moore, W.S., 1975. Sea level events and Pleistocene coral ages in the northern Bahamas. Quat. Res. 5, 215–224.
Omura, A., Maeda, Y., Kawana, T., Siringan, F.P., Berdin, R.D., 2004. U-series dates of Pleistocene corals and their implications to the paleo-sea levels and the vertical displacement in the Central Philippines. Quat. Int. 115–116, 3–13.
Ota, Y., Omura, A., 1992. Contrasting styles and rates of tectonic uplift of coral reef terraces in the Ryuku and Daito Islands, Southwestern Japan. Quat. Int. 15–16, 17–29.
Otto-Bliesner, B.L., Marshall, S.J., Overpeck, J.T., Miller, G.H., Hu, A., 2006. Simulating Arctic climate warmth and icefield retreat in the Last Interglaciation. Science 311, 1751–1753.
O'Leary, M.J., Hearty, P.J., Thompson, W.G., Raymo, M.E., Mitrovica, J.X., Webster, J.M., 2013. Ice sheet collapse following a long period of stable sea level during the Last Interglacial. Nat. Geosci. 6, 796–800.
Peltier, W.R., 2004. Global glacial isostasy and the surface of the ice-age Earth: the ICE-5G (VM2) model and GRACE. Annu. Rev. Earth Planet. Sci. 32, 111–149.
Potter, E.-K., Esat, T.M., Schellmann, G., Radtke, U., Lambeck, K., McCulloch, M.T., 2004. Suborbital-period sea-level oscillations during marine isotope substages 5a and 5c. Earth Planet. Sci. Lett. 225, 191–204.
Radtke, U., Schellmann, G., 2006. Uplift history along the Clermont Nose traverse on the west coast of Barbados during the last 500,000 years-implications for paleo-sea level reconstructions. J. Coast. Res. 22, 350–356.
Raymo, M.E., Mitrovica, J.X., 2012. Collapse of polar ice sheets during the stage 11 interglacial. Nature 483, 453–455.
Roberts, D.L., Karkanas, P., Jacobs, Z., Marean, C.W., Roberts, R.G., 2012. Melting ice sheets 400,000 yr ago raised sea level by 13 m: past analogues for future trends. Earth Planet. Sci. Lett. 357, 226–237.
Robinson, A., Calov, R., Ganopolski, A., 2011. Greenland ice sheet model parameters constrained using simulations of the Eemian interglacial. Clim. Past 7, 381–396.
Rowley, D.B., Forte, A.M., Moucha, R., Mitrovica, J.X., Simmons, N.A., Grand, S.P., 2013. Dynamic topography change of the eastern United States since 3 million years ago. Science 340, 1560–1563.
Schellmann, G., Radtke, U., 2004. A revised morpho- and chronostratigraphy of the Late and Middle Pleistocene coral reef terraces on Southern Barbados (West Indies). Earth Sci. Rev. 64, 157–187.
Schellmann, G., Radtke, U., Potter, E.-K., Esat, T.M., McCulloch, M.T., 2004. Comparison of ESR and TIMS U/Th dating of marine isotope stage (MIS) 5e, 5c, and 5a coral from Barbados—implications for palaeo sea-level changes in the Caribbean. Quat. Int. 120, 41–50.
Shackleton, N.J., 2000. The 100,000-year ice-age cycle identified and found to lag temperature, carbon dioxide, and orbital eccentricity. Science 289, 1897–1902.
Siddall, M., Rohling, E.J., Almogi-Labin, A., Hemleben, Ch, Meischner, D., Schmelzer, I., Smeed, D.A., 2003. Sea-level fluctuations during the Last Glacial cycle. Nature 423, 853–858.
Sieh, K., Natawidjaja, D.H., Meltzner, A.J., Shen, C.C., Cheng, H., Li, K.S., Suwargadi, B.W., Galetzka, J., Philibosian, B., Edwards, R.L., 2008. Earthquake supercycles inferred from sea-level changes recorded in the corals of west Sumatra. Science 322, 1674–1678.
Spasojević, S., Liu, L., Gurnis, M., Müller, R.D., 2008. The case for dynamic subsidence of the U.S. east coast since the Eocene. Geophys. Res. Lett. 35, L08305.
Speed, R.C., Cheng, H., 2004. Evolution of marine terraces and sea level in the Last Interglacial, Cave Hill, Barbados. Geol. Soc. Am. Bull. 116, 219–232.
Stein, M., Wasserburg, G.J., Aharon, P., Chen, J.H., Zhu, Z.R., Bloom, A., Chappell, J., 1993. TIMS U-series dating and stable isotopes of the Last Interglacial event in Papua New Guinea. Geochim. Cosmochim. Acta 57, 2541–2554.
Stone, E.J., Lunt, D.J., Annan, J.D., Hargreaves, J.C., 2013. Quantification of the Greenland ice sheet contribution to Last Interglacial sea level rise. Clim. Past 9, 621–639.

Thompson, W.G., Curran, H.A., Wilson, M.A., White, B., 2011. Sea-level oscillations during the Last Interglacial highstand recorded by Bahamas corals. Nat. Geosci. 4, 684–687.
Thurber, D.L., Broecker, W.S., Blanchard, R.L., Potratz, H.A., 1965. Uranium-series ages of Pacific atoll coral. Science 149, 55–58.
Vaughan, D.G., et al., 2013. Observations: Cryosphere. In: Stocker, T.F., et al. (Eds.), Climate Change 2013: the Physical Science Basis. Contribution of Working Group I to the Fifth Assessment Report of the Intergovernmental Panel on Climate Change. Cambridge University Press, Cambridge, United Kingdom and New York, NY, USA.
Veeh, H.H., 1966. Th^{230}/U^{234} and U^{234}/U^{238} ages of Pleistocene high sea level stand. J. Geophys. Res. 71, 3379–3386.